RESEARCH Open Access



Baculovirus-mediated production and purification of ferritin nanoparticles for rift valley fever vaccine development

Margarida Q. Rodrigues^{1,2}, Ashni Tambaclal^{1,2}, Brian Kloss³, Paula M. Alves^{1,2} and António Roldão^{1,2*}

Abstract

Background Rift Valley fever (RVF) is a WHO-prioritized zoonotic, vector-borne disease with no licensed prophylaxis available for humans, highlighting the need for effective vaccine strategies. Nanoparticle-based platforms for antigen presentation offer a promising approach for vaccine development.

Results In this work, we engineered ferritin (Ft) nanoparticles to display the immunogenic Gn domain of RVF virus (GnFt) and systematically assessed the production, purification, and physico-chemical properties of the purified nanoparticles. Baculovirus-based expression systems were evaluated in insect (*Sf*9, High-Five™, *Tn*ao38, and *Tn*ms42) and mammalian cells (HEK293 and CHO), revealing *Sf*9 cells as the most efficient host for producing GnFt nanoparticles. In addition, affinity-based chromatography was explored, yielding GnFt nanoparticles of > 95% purity (as assessed by SDS-PAGE) and an overall production yield of 0.2 mg/L culture. Biophysical characterization (e.g., high-performance liquid chromatography, dynamic light scattering, electron microscopy, and mass photometry) confirmed proper 24-mer nanoparticle assembly (1,344 kDa and 20 nm) and structural integrity. Binding affinity to Gn-targeting monoclonal antibodies was demonstrated by biolayer interferometry, with dissociation constants in the nM range, indicating retained antigenic functionality.

Conclusions These findings demonstrate the successful development of a platform for producing structurally stable, pure, and functional Gn-presenting ferritin nanoparticles, supporting their potential use for RVF vaccine development.

Background

Protein-based vaccines use antigens derived from pathogens, representing a safer alternative to live or attenuated vaccines. When these antigens are displayed on nanoparticles, they become more effective than soluble subunits by mimicking the natural size of pathogens [1], thereby triggering a stronger immune response [2].

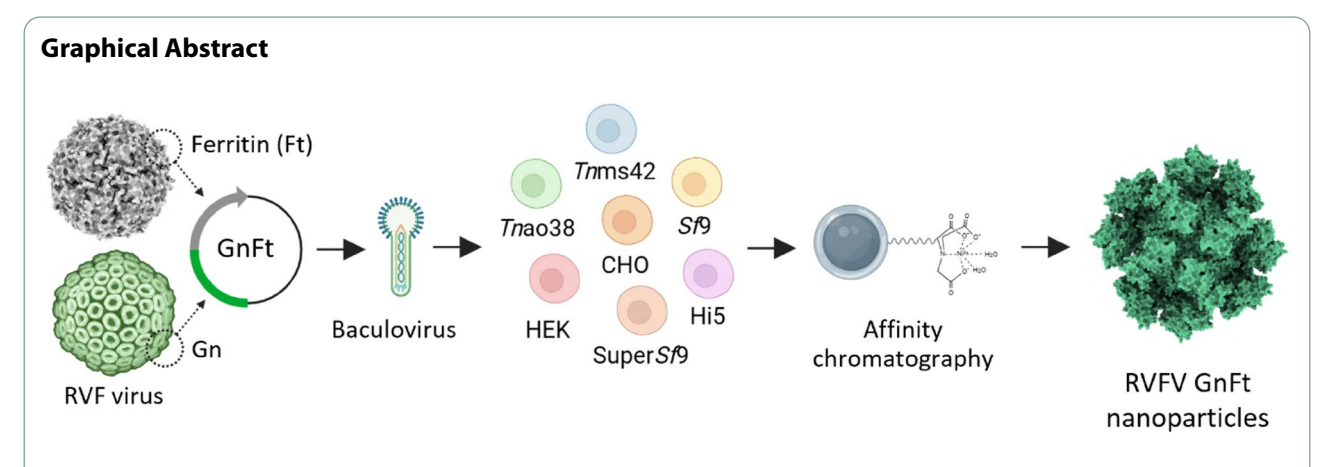
*Correspondence: António Roldão aroldao@ibet.pt

Full list of author information is available at the end of the article

Among various nanoparticle platforms, the 24-mer ferritin nanoparticle stands out for its safety, self-assembly, stability, and biocompatibility, making it a promising platform for vaccine development [3]. Antigens can be presented on ferritin by bioconjugation, such as tag/catcher technology [4], click chemistry [5], and enzymatic catalysis [6], allowing proteins to maintain their native conformation and function. However, bioconjugation adds complexity to the bioprocess, with desirable conjugation efficiencies being seldom obtained. Consequently, most ferritin-based vaccines are produced by genetically fusing the genes coding for ferritin and the antigen [7]. This strategy has led to candidates advancing



© The Author(s) 2025, corrected publication 2025. **Open Access** This article is licensed under a Creative Commons Attribution-NonCommercial-NoDerivatives 4.0 International License, which permits any non-commercial use, sharing, distribution and reproduction in any medium or format, as long as you give appropriate credit to the original author(s) and the source, provide a link to the Creative Commons licence, and indicate if you modified the licensed material. You do not have permission under this licence to share adapted material drived from this article or parts of it. The images or other third party material in this article are included in the article's Creative Commons licence, unless indicated otherwise in a credit line to the material. If material is not included in the article's Creative Commons licence and your intended use is not permitted by statutory regulation or exceeds the permitted use, you will need to obtain permission directly from the copyright holder. To view a copy of this licence, visit http://creativecommons.org/licenses/by-nc-nd/4.0/.



Keywords Ferritin nanoparticles, Nanoparticle-based vaccines, Antigen display, Recombinant protein expression, Baculovirus expression system

to clinical trials against influenza [8–10], Epstein-Barr virus [11], SARS-CoV-2 [12], and HIV [13].

Genetic fusion has limited attachment points at the Nor C-termini, while folding issues and steric hindrance can interfere with proper nanoparticle assembly and affect productivity. These challenges can be mitigated through in silico conformation prediction and design of engineered proteins and linkers. Yet, experimental validation remains essential to fully realize the potential of ferritin nanoparticles as vaccine candidates.

Bacterial systems were initially used to produce peptide-fused ferritin nanoparticles [7]. As interest in presenting more complex antigens grew, mammalian cells (e.g., Human embryonic kidney [HEK] and Chinese hamster ovary [CHO]) and, to a lesser extent, insect cells (e.g., Sf9), have become the preferred expression systems for ferritin-based vaccines (reviewed in [3]). These systems avoid the challenges associated with refolding proteins from bacterial inclusion bodies [14] and enable post-translational modifications typical of eukaryotic cells.

The insect cell-baculovirus expression vector system (IC-BEVS) has become an established platform for producing biologics, with successful products commercially available, like Cervarix® [15] and Flublok® [16]. This system is based on the natural infectiosity and self-replicating capacity of baculoviruses in insect cells. Upon infection, new virus generation coincides with recombinant expression of the protein of interest. Baculoviruses can also transduce mammalian cells [17] (termed Bac-Mam), enabling transgene expression when an appropriate promoter, such as the cytomegalovirus (CMV) promoter, is present [18]. This system is non-replicative in mammalian cells and requires a higher concentration of starting baculovirus since mammalian cells are not their natural host.

Rift Valley fever (RVF) is a WHO-prioritized vectorborne zoonotic disease caused by RVF virus (RVFV). Recurrent outbreaks occur in ruminants and humans in sub-Saharan Africa and the Arabian Peninsula [19], with significant societal and economic impacts. RVF is mainly controlled in livestock using live-attenuated or inactivated viruses [20]; however, no licensed vaccine is available for human use, and safe veterinary vaccines are still needed. Existing live-attenuated vaccines are associated with teratogenicity and residual virulence in ruminants, while inactivated vaccines require multiple dosing [21, 22]. From a biomanufacturing point of view, as a Biosafety Level 3 (BSL-3) pathogen, the development of live-attenuated/inactivated virus vaccines requires viral expansion and manipulation in BSL-3 facilities, being more hazardous than to develop next-generation vaccines platforms (e.g., mRNA, viral vectors, VLPs, subunit vaccines).

RVFV glycoproteins Gn and Gc, are involved in cell attachment and virus-cell membrane fusion and considered major antigenic components of the viral membrane [23]. Neutralizing antibodies predominantly target the Gn protein [24], making it an ideal candidate for next-generation vaccine development. In this work, we establish a process for producing ferritin nanoparticles that display the RVFV Gn head domain as a vaccine candidate. We optimized and compared the IC-BEVS and BacMam systems in terms of productivity and product quality and implemented a purification process that achieves greater than 95% purity.

Methods

Construct design and expression vectors The N-terminal extension of bullfrog (*Rana catesbeiana*) ferritin lower subunit (res. 2–9, PDB ID: 1RCC [25]) with a point mutation N8Q to eliminate a potential *N*-glycosylation site

was fused to *Helicobacter pylori* ferritin (res. 3-167, PDB ID: 3BVE [26]) with point mutations I7E to preserve the conserved salt bridge with bullfrog ferritin at residue 6R, and N19Q to remove a potential *N*-glycosylation site; this hybrid ferritin was previously designed by Kanekiyo et al. [11] to have antigen-presentation sites evenly distributed across its surface.

The Gn head domain sequence (res. 154-467, Uni-Prot ID: P03518 [27]) was selected with point mutations E276G, L329H and I444V [28] and fused upstream to the hybrid ferritin using a glycine-serine (GS)-rich linker. The resulting Gn-ferritin (GnFt) nucleotide sequence was codon-optimized for expression in insect and mammalian cells, using GenSmart Codon Optimization (GenScript). For secretion into the culture medium, N-terminal signal peptides from Autographa californica nuclear polyhedrosis virus major envelope glycoprotein (GP67) and human interleukin-2 (IL2) were used for insect and mammalian cells, respectively. An alanine residue was added downstream the signal peptides, followed by a hexahistidine tag to facilitate purification, resulting in two constructs: GP67-A-GnFt and IL2-A-GnFt. These sequences were synthesized and cloned into the pUC-GW-Kan expression vector (Azenta).

The synthesized sequences were further cloned into two different ligation-independent cloning (LIC)-adapted expression vectors [29]. GP67-A-GnFt was inserted into pFastBac C-term [30] for expression in insect cells, resulting in pFastBac-GP67-A-GnFt. Similarly, IL2-A-GnFt was inserted into the pBacMam C-term [30, 31] for expression in mammalian cells, yielding pBacMam-IL2-A-GnFt. Site-directed mutagenesis was performed to generate constructs lacking the alanine residue, resulting in pFastBac-GP67-GnFt and pBacMam-IL2-GnFt. All plasmids were transformed into DH10B-T1 competent cells (Thermo Fisher Scientific) and purified using E.Z.N.A.® Plasmid DNA Mini Kit I (Omega Bio-tek).

Additionally, dsDNA coding for human cluster of differentiation 5 (hCD5) and bovine prolactin (bPRL) signal sequences were synthesized by IDT and used to replace the IL2-A sequence in pBacMam-IL2-A-GnFt using InFusion® cloning (Takara), generating the vectors pBacMam-hCD5-GnFt and pBacMam-bPRL-GnFt. Further modifications involved extracting the human phosphoglycerate kinase (PGK) promoter and the enhanced green fluorescent protein (EGFP) sequences from the pRRLSIN.cPPT.PGK-GFP.WPRE vector and ing them downstream of the GnFt coding sequence in pBacMam-hCD5-GnFt using InFusion® cloning, resulting in pBacMam-hCD5-GnFt-PGK-EGFP. This modification was intended to assess mammalian transduction via fluorescence-based methods. Final vectors were transformed into Stellar[™] competent cells (Takara) according to the manufacturer's instructions and purified using the GeneJET Plasmid Miniprep Kit. Primer sequences used for LIC, mutagenesis, and InFusion® cloning are detailed in Table S1. Signal peptide and protein constructs, including their corresponding amino acid sequences, are provided in Table S2.

For bacmid generation by transposition [32], donor plasmids were transformed into DH10EmBacY (Geneva Biotech) or MAX Efficiency™ DH10Bac (Gibco) competent cells. Bacmids were extracted using reagents from the miniprep kits, followed by precipitation with ethanol/isopropanol, resuspension in water, and storage at -20 °C until further use.

DNA concentration was determined spectrophotometrically at 260 nm using a Nanodrop OneC (Thermo Fischer Scientific).

Cell lines and culture media Insect cell lines Sf9 (Invitrogen), SuperSf9-2 (SuperSf9, OET), High Five™ (Hi5, Gibco), Hi5-derivatives Tms42 [33, 34] and BTI-Tnao38 (Tnao38) [35, 36], and mammalian cell lines HEK293-6E (HEK293, NRC Canada) and FreeStyle™ CHO-S cells (CHO, Gibco) were passaged every 2–3 days in 125 mL−2 L shake flasks (Corning) with a working volume of 10–20%.

Insect cells were maintained at 27 °C in an Inova 44R shaking incubator (Eppendorf) set to 100 rpm using Sf-900 $^{\text{m}}$ II SFM (Sf900II) or Express Five $^{\text{m}}$ SFM supplemented with 20 mM L-Glutamine (for Hi5 only). Mammalian cell lines were maintained at 37 °C in a humidified atmosphere with 5% CO₂ in a Multitron shaking incubator (Infors HT) set to 100 rpm. HEK293 were grown in FreeStyle $^{\text{m}}$ F17 Expression Medium supplemented with 4 mM GlutaMAX $^{\text{m}}$, 0.1% Pluronic $^{\text{m}}$ F-68 and 25 µg/ml Geneticin $^{\text{m}}$, while CHO were cultivated in CD CHO Medium supplemented with 8 mM GlutaMAX $^{\text{m}}$ (all from Gibco).

Viable cell density (VCD) and cell viability were assessed using the trypan-blue exclusion method with a Cedex HiRes cell analyser (Roche) following the manufacturer's instructions.

Baculovirus generation, amplification and storage *Sf*9 cells (2 mL) were seeded at 0.5×10^6 cells/mL in 6-well culture plates and allowed to adhere. For each transfection reaction, 8 μl of Cellfectin[™] II (Gibco) and 1 μg of bacmid DNA were diluted in 200 μl of *Sf*9 medium and incubated at room temperature (RT) for 30 min. Medium in the culture plates was aspirated and replaced with 1.8 mL of fresh medium, along with the transfection mixture. After 96 h of incubation at 27 °C, the recombinant baculovirus (rBAC) P0 was harvested. For rBAC amplification, *Sf*9 cells were infected at 1×10^6 cell/mL using varying dilutions of virus. rBAC were harvested by centrifugation ($200 \times g$, $10 \min + 2,000 \times g$, $20 \min$, 4 °C) when viabil-

ity reached 80–90%, typically after 3–4 days. rBAC stocks were amplified up to P2 and stored at $4\,^{\circ}\text{C}$ in the dark until further use.

For BacMam applications, certain rBAC stocks were concentrated using PEG precipitation method. Briefly, rBAC stocks were mixed with 20% (w/v) PEG 8000 solution to a final concentration of 2% (v/v). The mixture was incubated overnight on a roller mixer at 4 °C and centrifuged (3,200×g, 30 min, 4 °C). The resulting pellets were resuspended in PBS supplemented with 0.5 M sucrose using 1/10 to 1/100 of the starting volume.

Baculovirus infectious titers were determined by the MTT assay [37, 38].

Small-scale expression assay Expression assays were conducted in triplicate using 125-mL shake flasks with a working volume of 10–20%. Tested conditions included different cell lines, signal sequences, cell concentration at transduction/infection, multiplicities of infection (MOIs, defined as the number of plaque forming units (pfu) of virus per number of cells), media exchange, sodium butyrate (NaBut) concentration and timing of addition, and temperature shift. Samples were collected every 24 h to monitor VCD, cell viability, and GnFt production via western blot.

Comparison of GnFt expression in mammalian cells using established conditions of BacMam expression Mammalian cell cultures (HEK293 and CHO cells) were grown in triplicate in 50-mL (5 mL working volume) Corning® mini bioreactors and transduced at 1×10^6 cells/mL using rBAC containing the construct hCD5-GnFt-PGK-EGFP at three different MOIs: 2, 20, and 100 pfu/cell. Samples were collected every 24 h to monitor VCD, cell viability, and GnFt expression via western blot.

Purification using His+Bind resin Sf9, Hi5, and HEK293 cultures were grown in 2 L (250 mL working volume) shake flasks using established optimal conditions. Cell cultures were harvested by centrifugation (2,000×g, 20 min) and filtered (0.22 µm). Clarified supernatants were concentrated and dialysed 5× using 20 mM Tris, 500 mM NaCl, pH 7.5 (base buffer) and a 1000 kDa Pellicon® 2 Cassette with a Ultracel® membrane (Millipore) operated in tangential flow filtration (TFF) mode. The resulting retentates were filtered (0.22 μm), supplemented with 10 mM imidazole (final concentration), and incubated with 1-mL His. Bind resin® (Millipore) for 1 h at 4 °C in a roller mixer. Protein was purified using Econo-Pac® gravity chromatography columns (Bio-Rad). For Sf9 and Hi5 cells, wash and elution were performed with base buffer supplemented with 70 and 250 mM imidazole, respectively. For HEK293, a step gradient ranging 25-250 mM was used.

Purification using ProteIndex™ Ni-Penta™ prepacked cartridges Sf9 cells were grown in 2 L (200 mL working volume) shake flasks using established optimal conditions. Clarified supernatants were filtered (0.22 μm) and either directly loaded (DL) into 1-mL ProteIndex™ Ni-Penta™ agarose 6FF prepacked cartridges (Marvelgent Biosciences) or concentrated/dialysed by TFF as previously described. The resulting retentate was filtered (0.22 μm) to obtain the treated clarified (TC). Protein suspensions (DL and TC) were loaded at 1 mL/min onto a 1-mL ProteIndex™ cartridge, pre-equilibrated with base buffer, connected to an Äkta Explorer system (Cytiva). The column was washed with 20 mM imidazole, and elution performed using a 20-min linear gradient up to 250 mM imidazole.

Production of ferritin nanoparticles devoid of antigen The bullfrog-H. pylori hybrid ferritin (Ft) devoid of the Gn antigen contained a hexahistidine tag at the N-terminal and was synthesized and cloned into pOET1.1 (Oxford Expression Technologies) by GenScript. rBAC containing the Ft sequence was generated by homologous recombination using flashBAC ULTRA (Oxford Expression Technologies) as per manufacturer's instructions, and amplified as described above. Sf9 cultures were grown in 2 L (200 mL working volume) shake flasks and infected at 2×10^6 cell/mL and MOI of 1 pfu/cell. After 72 h, cell pellets were harvested by centrifugation and resuspended in base buffer supplemented with 0.2% Deviron® C16 (Merck), 50 U/mL Benzonase^o (Millipore), 2 mM MgCl₂, and cOmplete ™ protease inhibitor cocktail (Roche) using 1/10 of the starting volume. The suspension was incubated on a roller mixer for 30 min at 4 °C, followed by centrifugation (16,000×g, 1 h, 4 °C). The lysate was filtered (0.45 µm) and purified using a 1-mL ProteIndex™ cartridge as described above.

Protein storage and quantification After chromatography, GnFt- and Ft-containing fractions were pooled, concentrated, dialyzed against formulation buffer (20 mM Tris, 150 mM NaCl, pH 7.5) using 100-kDa cutoff Amicon° centrifugal units (Millipore), filtered (0.22 μ m), and stored at -80 °C. Protein concentration was estimated using Pierce[™] BCA protein assay kit (Thermo Scientific) or absorbance at 280 nm using the extinction coefficient $4.74 \times 10^4 \, \text{M}^{-1} \text{cm}^{-1}$ (GnFt, 1-mer) and $2.14 \times 10^4 \, \text{M}^{-1} \text{cm}^{-1}$ (Ft, 1-mer), as estimated by the ProtParam tool (Expasy [39]), in a Nanodrop OneC.

SDS-PAGE and western blot analysis Samples were mixed with LDS sample buffer and sample reducing agent, heated (3 min, 99 °C), loaded onto 4–12% bis-tris gels, and electrophoresis performed (40 min, 200 V, 400 mA) using MES SDS running buffer and SeeBlue™ Plus2 pre-stained

protein standard. Proteins were transferred onto nitrocellulose membranes using iBlot™ 2 transfer stacks and gel transfer device (10 min, 20 V) (all from Invitrogen).

After transfer, membranes were blocked for 1 h at RT in tris-buffered saline (Sigma-Aldrich) with 0.1% Tween-20 (Millipore) (TBST) containing 5% (w/v) skim milk (Millipore). Membranes were incubated overnight at RT with primary antibodies, followed by a 1 h incubation at RT with secondary antibodies; membranes were washed three times with TBST for 5 min between each incubation step. Bands were revealed using NBT/BCIP 1-Step (Thermo Fisher Scientific) and documented with an iBright FL1500 (Invitrogen).

Antibodies were prepared in blocking solution and included mouse monoclonal anti-RVFV Gn glycoprotein (NR-43185 [40], BEI Resources) and mouse 6x-HisTag monoclonal antibody (MA1-21315, Invitrogen) as primary antibodies (1:1,000–2,000) and goat anti-mouse IgG conjugated with alkaline phosphatase (A3438-25ML, Sigma-Aldrich) (1:5000) as secondary antibody.

Densitometry Densitometry analysis of protein bands on the western blot membranes was conducted using ImageJ software [41]. Relative volumetric titer for each sample was calculated by dividing the band intensity area of that sample by the intensity area of a given condition. Relative cell-specific productivity was determined similarly, with the intensity area further normalized by dividing it by the area under the VCD curve.

High performance liquid chromatography (HPLC) Samples were analysed on a HPLC system with a Vanquish Diode Array Detector (Thermo Scientific) using a Bio SEC-5 column (500 Å, 5 μm, 4.6×300 mm, Agilent) at a flow rate of 0.3 mL/min. Formulation buffer was used as mobile phase and BEH450 SEC Protein Standard Mix (Waters) as molecular weight standard.

Dynamic light scattering (DLS) The size distribution of particles in protein samples was estimated by DLS using a Zetasizer Ultra (Malvern Panalytical). Protein samples were diluted in formulation buffer to a final volume of 800 μ L and placed in disposable cuvettes. Each sample was measured three times, and data analysed using ZS Xplorer software (Malvern Panalytical).

Mass photometry The molecular mass of proteins was determined using the mass photometer SamuxMP (Refyne). Formulation buffer (18 μ L) was added to the slide and autofocus adjusted. Subsequently, 2 μ L of sample was resuspended in the buffer droplet. Data was acquired and analyzed using AcquireMP and Discover MP software (Refyne), respectively.

Negative staining transmission electron microscopy (nsTEM) and single-particle analysis Sample preparation and imaging of nanoparticles by nsTEM were performed at the Electron Microscopy Facility at CIC bio-GUNE. Purified proteins were prepared at 0.1–0.3 mg/mL in formulation buffer. Freshly glow-discharged CF400-Cu grids (EM Sciences) were incubated with an 8-μL droplet of each sample for 60 s and then transferred to an 8-μL MilliQ water droplet for 30 s. Grids were subsequently placed on a uranyl acetate droplet for two consecutive 30 s incubations, and left to dry prior to visualization; excess liquid was removed using Whatman paper after each incubation.

For imaging, grids were transferred into an EM-11,170 pentaholder (Gatan) and visualized on a JEM-1230 transmission electron microscope (JEOL) equipped with a LaB6 emission gun (FEG), operated at 100 kV, and spherical aberration of 2.0 mm. Digital images were recorded on a 4 K×4 K (15 μm pixels) Ultrascan4000 $^{\!\!\!\!\!^{\text\tiny M}}$ charge-coupled device camera (Gatan) using a nominal magnification of 40,000 × (2.9 Å/pixel) with a total dose on the order of 40–60 electrons/Å 2 per exposure, at defocus values ranging from 3.0 to 5.0 μm .

Single-particle analysis was performed using Cryo-SPARC v4.3 [42]. From 35 micrographs, 131,071 and 47,020 particles were extracted for Ft and GnFt, respectively, using a template picker. After four rounds of 2D classification, the final 2D classes contained 10,820 Ft and 2,888 GnFt nanoparticles.

Biolayer interferometry (BLI) of antibodies binding to nanoparticles Nanoparticle binding to Gn-specific monoclonal antibodies was measured with an Octet RED96 (FortéBio). NTA biosensors (Sartorius) were equilibrated in kinetic buffer (Sartorius) for 180 s, loaded with GnFt or Ft nanoparticles (10 μ g/mL) for 300 s, and subjected to three-fold serial antibody dilutions (starting at 90 nM) for 600 s association and 600 s dissociation in kinetic buffer. Regeneration between experiments was achieved with glycine (100 mM, pH 2.0) followed by nickel recharging with NiSO₄ (100 mM). Kinetic constants were determined by fitting data to a non-linear regression model in GraphPad Prism v10.4.2. Antibodies included monoclonal anti-RVFV Gn NR-43185, NR-43189, NR-43190, and NR-43195 (BEI Resources).

Statistical analysis Statistical analysis and graphical representation were performed using GraphPad Prism v10.4.1. To determine statistical significance, unpaired t-test was used for comparisons between two groups. For multiple groups, one- or two-way analysis of variance (ANOVA) followed by Tukey's or Šídák's multiple comparisons test was employed. A *p*-value greater than 0.05 was considered non-significant (ns). Significance levels

are indicated as follows: *p<0.05, **p<0.01, *** p<0.001, **** p<0.0001. Results are displayed as mean ± standard deviation (SD).

Results

BacMam system for producing GnFt nanoparticles

To explore the BacMam system for GnFt nanoparticle production, two mammalian cell lines were initially compared: HEK293 and CHO cells; cells were infected at a viable cell density (VCD) of 2×10^6 cells/mL with 10% (v/v) rBAC $_{\rm IL2-A}$ formulated in *Sf*9 insect cell culture medium (Sf900II). After 96 h, expression of GnFt was only detectable by western blot in culture supernatant of HEK293 cells (data not shown).

To determine whether residual components from Sf900II, used during rBAC amplification, had any influence on GnFt expression, particularly given the high multiplicity of infection (MOI) required for mammalian cell transduction, strategies such as exchanging the cell culture medium upon transduction or using concentrated rBAC stocks resuspended in PBS buffer were evaluated. For these experiments, HEK293 cells were transduced at 2×10^6 cells/mL with rBAC_{IL2-A} and MOI of 25 pfu/cell. Initial results show that complete media exchange (to HEK293 cell growth medium) at 6 hours post-infection (hpi) has no detrimental effects on GnFt expression, with cell growth and viability profile comparable to that of non-infected cells (Fig. S1A, B). Media exchange at 1, 3, and 6 hpi was further investigated. Although the uptake of infectious virus increased over time, no significant difference in cell growth kinetics nor GnFt expression was observed (Fig. S1C, D, E). Therefore, to streamline the procedure, media exchange at 3 hpi was selected as best strategy. To eliminate the need for media exchange, rBAC stocks were concentrated and stored in PBS supplemented with 0.5 M sucrose (PBS/Suc), and subsequently evaluated for HEK293 transduction and GnFt expression. This approach yielded growth kinetics comparable to non-infected cells and resulted in productivity levels similar to those achieved with rBAC formulated in Sf900II medium followed by media exchange at 3 hpi (Fig. S1F, G). Overall, these findings suggest that both strategies (i.e., media exchange at 3 hpi or concentrated rBAC) are suitable to limit any potential impact that residual components from Sf900II medium may have on HEK293 transduction and subsequently on GnFt expression.

The next set of experiments focused on improving GnFt expression in HEK293 cells, exploring different signal peptides, MOI, VCD, additives, and culture temperature. Various signal sequences were tested: IL2, hCD5 and bPRL, which have been used for extracellular production of antigen-fused ferritin nanoparticles in mammalian cells (reviewed in [3]). The IL2 sequence with an adjacent alanine residue (IL2-A) was also compared

(Fig. 1A), which was previously shown to improve protein secretion [43]. Although secretion was similar among the constructs, ${\rm rBAC_{hCD5}}$ resulted in the highest extracellular-to-intracellular GnFt protein ratio (Fig. 1B) and was selected for subsequent studies.

Transduction optimization followed by evaluating different cell concentrations at transduction (1 and 2×10^6 cells/mL), MOIs (10, 25, and 50 pfu/cell) and times of harvest (TOH: 72 and 96 hpi). Expression was similar across all conditions using an initial concentration of 1×10^6 cells/mL (Fig. 1C). However, using 2×10^6 cells/mL as a starting point, significantly higher expression was observed for MOIs of 25 or 50 pfu/cell and TOH of 96 hpi (Fig. 1D). Since MOI of 25 pfu/cell requires less viral content, subsequent experiments were conducted using a concentration at transduction of 2×10^6 cells/mL, MOI of 25 pfu/cell, and TOH of 96 hpi.

Given that histone deacetylase inhibitors, such as sodium butyrate (NaBut), are known to increase protein expression in mammalian cells, different concentrations of NaBut (0, 1, and 5 mM) and timings of addition (8 and 24 hpi) were tested. NaBut supplementation increased GnFt expression, with no statistically significant difference between 1 and 5 mM. Notably, adding NaBut at 8 hpi resulted in higher expression compared to 24 hpi (Fig. 1E). Since NaBut's cytotoxicity led to decreased cell viability when added at 8 hpi (Fig. S2D, E), 1 mM NaBut supplementation was selected to minimize its negative impact.

Mild hypothermia is known to reduce cell growth rates while increasing productivity in mammalian cells [44, 45]. To test this, HEK293 cells were cultured at 30 °C following NaBut supplementation. As expected, growth arrest was observed compared to cells grown at 37 °C (Fig. S2F). Although no difference in volumetric GnFt titer was observed between the two temperatures, the lower VCD achieved at 30 °C led to a higher cell-specific productivity, particularly after 96 hpi (Fig. 1F). Nonetheless, to streamline the procedure, standard HEK293 cell culture temperature (37 °C) was maintained.

Finally, the optimal expression condition herein identified (i.e., concentrated rBAC_{hCD5}, 1 mM NaBut supplementation at 8 hpi) was compared to the initial condition (i.e., rBAC_{hCD5} formulated in Sf900II, medium exchange at 3 hpi); in both, HEK293 were transduced at an initial concentration of transduction of 2×10^6 cells/mL, MOI of 25 pfu/cell, and cultured at 37 °C. The optimized condition resulted in a 5.4-fold volumetric titer and a 7.5-fold cell-specific productivity increase (Fig. 1G).

The best condition identified above was used to reassess the potential of HEK293 and CHO cells for GnFt expression. In this experiment, cells were transduced with ${\rm rBAC_{hCD5_GFP}}$ at 1×10^6 cells/mL, using MOIs of 2, 20, and 100 pfu/cell, and 1 mM NaBut added at 8

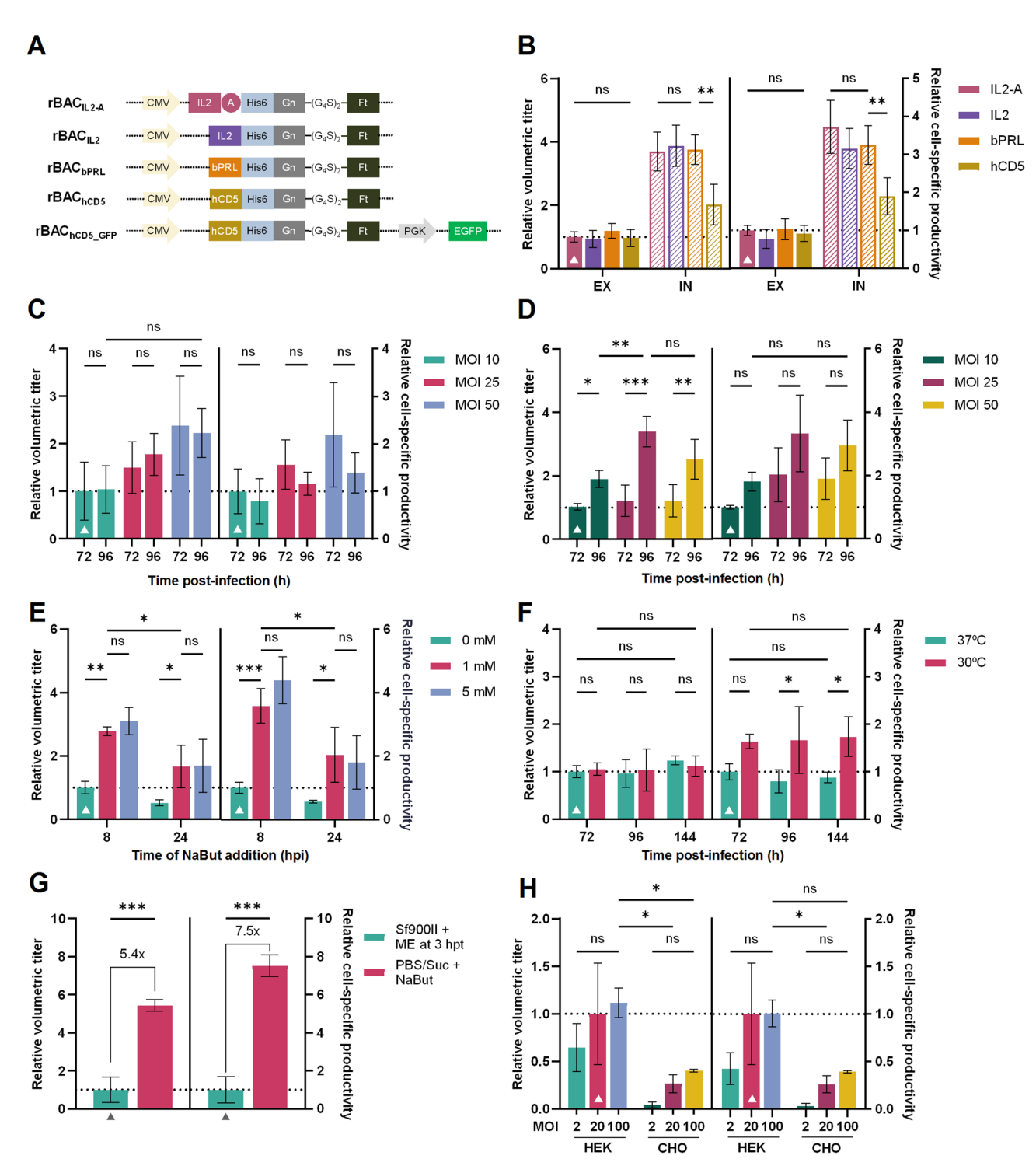


Fig. 1 Optimization of the BacMam system for producing GnFt. (**A**) Overview of BacMam rBAC constructs. (**B-H**) Analysis of various conditions on the volumetric titer (left) and cell-specific productivity (right) of GnFt following rBAC transduction of HEK293 cells. (**B**) Effect of different signal sequences (IL2-A, IL2, bPRL, hCD5) on GnFt secretion; rBAC_{hCD5} construct was selected for subsequent experiments; EX and IN stand for extracellular and intracellular environments, respectively. (**C-D**) Impact of different MOIs (10, 25, 50 pfu/cell) on GnFt expression at 72 and 96 hpi in HEK293 cells transduced at (**C**) 1 or (**D**) 2×10^6 cells/mL. (**E**) Effect of NaBut concentration (0, 1, 5 mM) and timing of addition (8 and 24 hpi). (**F**) Effect of temperature after 1 mM NaBut addition at 8 hpi; cells were maintained at 37 °C or 30 °C. (**G**) Comparison of GnFt expression under optimized conditions (concentrated rBAC_{hCD5} and 1 mM NaBut added at 8 hpi [PBS/Suc + NaBut]) versus initial infection conditions (rBAC_{hCD5} formulated in Sf900II with media exchange at 3 hpi [Sf900II + ME at 3 hpi]). In panels (B), and (E-G) HEK293 cells were transduced at 2×10^6 cells/mL and MOI of 25 pfu/cell. (**H**) GnFt expression in HEK293 and CHO cells transduced with rBAC_{hCD5_GFP} at 1×10^6 cells/mL, using MOIs of 2, 20, and 100 pfu/cell, and 1 mM NaBut added at 8 hpi. In (B-H) GnFt expression was quantified by western blot densitometry using antibody against Gn, and are represented in relation to the condition marked by triangles (Δ). Data are presented as mean ±SD from n = 3 experimental replicates

hpi. Transduction was confirmed by detection of green coloured cells using fluorescence microscopy (data not shown), and GnFt expression was assessed at 96 hpi. No significant differences in GnFt expression were observed across different MOIs in each cell line, with expression in HEK293 being significantly higher than in CHO cells (Fig. 1H).

IC-BEVS to produce GnFt nanoparticles

As a starting point for optimizing GnFt production using IC-BEVS, the GP67 signal sequence was selected for secretion and compared with a construct containing an adjacent alanine residue (GP67-A) to assess any improvement in secretion efficiency (Fig. 2A). Sf9 cells were infected at 1×10^6 cells/mL and MOI of 0.1 pfu/cell. No significant differences were observed in volumetric or cell-specific secretion (Fig. 2B), nor in cell growth kinetics (Fig. S3); rBAC_{GP67-A} was selected for subsequent studies

To identify the best expression host, five insect cell lines were evaluated: *Sf*9, Super*Sf*9, Hi5, *Tn*ms42, and *Tn*ao38, using different cell concentrations at infection

(CCIs: 1 and 2×10⁶ cells/mL) and MOIs (0.1 and 1 pfu/ cell). For both Sf9 and SuperSf9, no significant difference in volumetric titer was observed across all tested conditions; on the other hand, cells infected at a CCI of 1×10^6 cells/mL exhibited higher cell-specific productivity compared to those infected at a CCI of 2×10^6 cells/ mL (Fig. S4A, B). These results, combined with the fact that lower CCIs minimize media component depletion and by-products accumulation, led to the selection of CCI of 1×10^6 cells/mL as best condition. As to MOI, 0.1 pfu/cell was selected for Sf9 cells to minimize rBAC stock usage, while 1 pfu/cell was considered optimal for SuperSf9 cells. Products derived from IC-BEVS should be harvested at high cell viabilities (ideally>70%) to minimize the downsides of this lytic system, which occurred at 72 hpi, thus defined as the TOH.

For Hi5, Tnao38, and Tnms42, CCI of 1×10^6 cells/mL was globally considered advantageous over CCI of 2×10^6 cells/mL in terms of volumetric titer and cell-specific productivity. Regarding MOI, while 1 pfu/cell led to highest expression in Hi5 cells, no significant difference in productivity was observed between the different MOIs

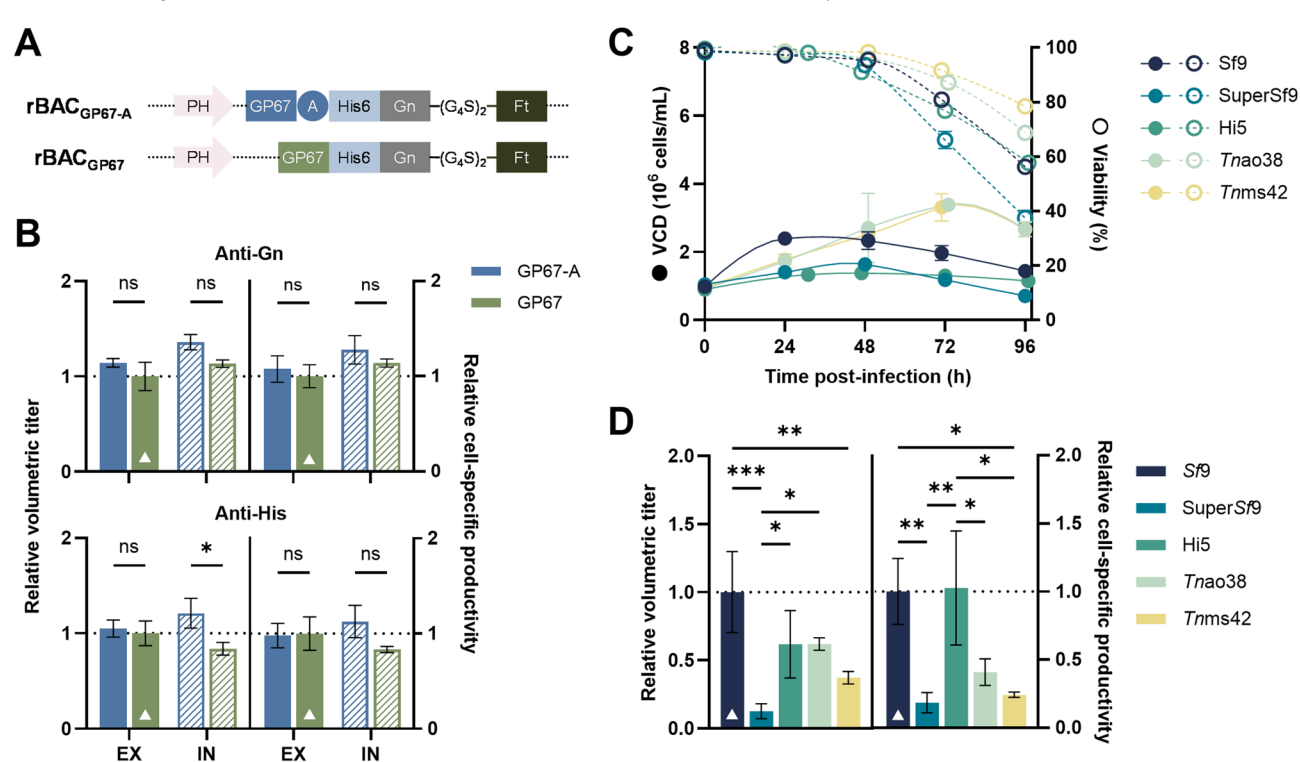


Fig. 2 Optimization of the IC-BEVS system for producing GnFt. (A) Overview of IC-BEVS rBAC constructs used in expression assays. (B-D) Analysis of various conditions on cell growth kinetics and GnFt nanoparticle productivity following infection of insect cells. (B) Effect of different signal sequences (GP67-A, GP67) on GnFt secretion in Sf9 cells infected at 1 × 10⁶ cells/mL and MOI of 0.1 pfu/cell. Volumetric titer (left) and cell-specific productivity (right) were assessed by western blot using antibodies against Gn (top) and histidine tag (bottom); rBAC_{GP67-A} construct was selected for subsequent experiments; EX and IN denote extracellular and intracellular environments, respectively. (C-D) Comparison of optimal conditions for each cell line: Sf9, Tnao38, and Tnms42 were infected at 1 × 10⁶ cells/mL and MOI of 0.1 pfu/cell, and SuperSf9 and Hi5 at 1 × 10⁶ cells/mL and MOI of 1 pfu/cell. (C) Viable cell density (VCD, a) and cell viability (O) kinetics. (D) Volumetric titer (left) and cell-specific productivity (right) of GnFt, quantified by western blot densitometry using antibody against histidine tag of samples from 72 hpi (Sf9, SuperSf9, Hi5) and 96 hpi (Tnao38, Tnms42). Data on bar charts are represented in relation to the condition marked by triangles (Δ). Data are presented as mean ± SD from n = 3 experimental replicates

for Tnao38 and Tnms42, thus MOI of 0.1 pfu/cell was chosen for these cell lines to reduce rBAC stock usage. Notably, productivity was negligible across all cell lines using CCI of 2×10^6 cells/mL and MOI of 0.1 pfu/cell (Fig. S4C, D, E). Regarding TOH, 72 hpi was selected for Hi5, while 96 hpi was selected for Tnao38 and Tnms42. A summary of the optimal infection conditions for each cell line using IC-BEVS is provided in Table 1.

The optimal infection conditions for each cell line were compared in terms of infection kinetics and productivity (Fig. 2C, D). *Sf*9 and Hi5 exhibited the highest volumetric titer and cell-specific productivity, suggesting these are the most promising cell lines for producing GnFt using IC-BEVS.

Purification of GnFt nanoparticles using immobilized metal affinity chromatography (IMAC)

Until this point, GnFt expression was assessed in cell culture bulk samples. To evaluate the quality attributes of GnFt nanoparticles, purification is necessary. For this purpose, a histidine tag was introduced at the N-terminal of GnFt to enable purification via IMAC.

Using the optimal expression conditions for Sf9, Hi5, and HEK293 cells identified in previous sections, clarified culture supernatants were buffer-exchanged by tangential flow filtration (TFF) followed by gravity chromatography purification using His+Bind resin. SDS-PAGE and western blot analysis revealed that GnFt protein from Sf9 cells was mostly secreted, contrarily to Hi5 and HEK293 cells in which GnFt protein remained mostly intracellular (Fig. S5). Additionally, Sf9-derived GnFt protein exhibited strong affinity for nickel-bound resin, with negligible presence in the flowthrough and wash fractions, and demonstrated high purity in the eluted fraction (Fig. S5). In contrast, GnFt derived from Hi5 and HEK293 cells could not be obtained in measurable amounts in the elution fractions (Fig. S5). Based on these results, only Sf9 cells were selected for further exploration of GnFt nanoparticle purification processes.

Aiming to establish a robust, scalable GnFt nanoparticle purification process, ProteIndex Ni-Penta prepacked cartridges were evaluated due to their compatibility with flow chromatography and their chemical stability, which theoretically allows for direct loading of clarified culture

Table 1 Summary of the optimal conditions for each cell line using IC-BEVS

	Sf9	SuperSf9	Hi5	Tnao38	Tnms42
CCI (x10 ⁶ cells/mL)	1	1	1	1	1
MOI (pfu/cell)	0.1	1	1	0.1	0.1
TOH (hpi)	72	72	72	96	96
Cell viability at TOH (%)	81 ± 2	66±3	77 ± 1	69±1	79±1

CCI: cell concentration at infection, MOI: multiplicity of infection, TOH: time of harvest

supernatants without prior buffer exchange. This contrasts with conventional nickel-based IMAC resins where nickel leaching mediated by cell culture media components can hinder purification. To test this hypothesis, two strategies were compared: loading of treated clarified (TC) supernatants (i.e., with prior buffer-exchange by TFF) and direct loading (DL) of clarified supernatants onto the ProteIndex cartridges.

Sf9 cells were infected at CCI of 2×10^6 cells/mL and MOI of 1 pfu/mL. Cell cultures were harvested at 72 hpi and subsequently processed for GnFt nanoparticle purification by flow IMAC (Fig. S6A). During elution, GnFt protein was detected at the same imidazole concentration in both TC and DL conditions, with comparable absorbance values, indicating similar protein capture efficiency. Importantly, a single elution peak was observed, enriched in GnFt (Fig. S6B). SDS-PAGE and western blot analysis showed the presence of GnFt in the DL wash fractions, which was not observed in the TC condition (Fig. S6C), suggesting that dialysis prior to column loading enhances the binding performance of ProteIndex cartridges.

Reducing SDS-PAGE analysis confirmed>95% purity of monomeric GnFt at the expected molecular weight of 56 kDa (Fig. 3A), with productivities of 0.2 mg/L culture for both purification strategies (Fig. 3B). The purified GnFt nanoparticles were further characterized using native-based analytics. DLS analysis showed that most nanoparticles purified by the TC strategy had an average size of 20 nm (Fig. 3C), representing the size of ferritin nanoparticles displaying Gn antigens. In contrast, the DL sample contained molecules with diameters ranging from 100 to 200 nm, indicative of the presence of large impurities such as vesicles, residual baculoviruses, or protein aggregates.

HPLC analysis of TC and DL samples showed overlapping elution curves at approximately 8.5 min, corresponding to 24-mer GnFt nanoparticles (Fig. 3D). The TC sample exhibited a single peak, suggesting this purification strategy effectively yields a homogeneous final product in the desired 24-mer conformation. In contrast, the DL sample contained a second, more pronounced peak located in the column void volume (i.e., beyond the maximum range of the Bio SEC-5 column) corresponding to large entities (>5 MDa), and consistent with the DLS results.

Noteworthy, three peaks eluted at 10, 13, and 16 min were visible in the DL strategy chromatogram, with the 13 min peak also visible for the TC approach. These peaks were not visible in the standard protein mix chromatogram, so they are not derived from column artefacts or the running buffer. Most likely, the peaks represent impurities from the *Sf*9 cell culture, as these are common to both treated clarified (TC) and direct loading

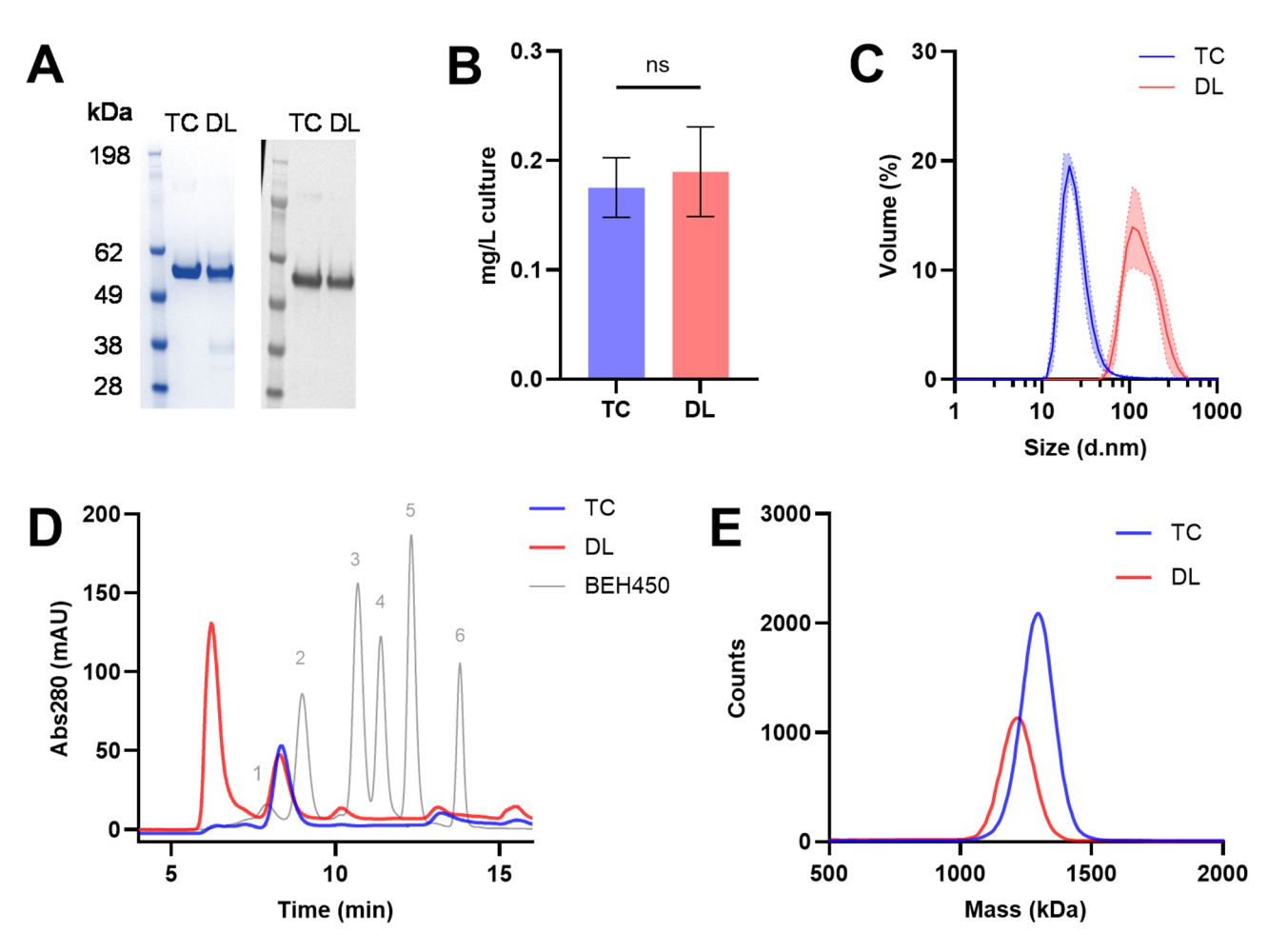


Fig. 3 Characterization of GnFt nanoparticles produced in *Sf9* and purified using ProteIndex Ni-Penta prepacked cartridges. (**A-E**) Characterization of purified GnFt nanoparticles obtained from different sample preparation: treated clarified (TC, blue) and direct load of clarified (DL, red). (**A**) SDS-PAGE (left) and western blot analysis using an antibody against Gn (right); wells contain 1 μ g of protein. (**B**) Production yield estimated by BCA protein assay. Data are presented as mean \pm SD from n=4 technical replicates. (**C**) Particle size distribution by DLS. Data represents mean \pm SD from n=3 technical replicates. Corresponding correlograms are presented in Fig. S7A. (**D**) HPLC analysis of 100- μ L samples at 1 μ M. BEH450 protein standard mix is represented in grey: (1) thyroglobulin dimer (1.4 MDa), (2) thyroglobulin (669 kDa), (3) IgG (150 kDa), (4) BSA (66.4 kDa), (5) myoglobin (17 kDa), (6) uracil (112 Da). (**E**) Molecular weight estimation by mass photometry

(DL) purification strategies. These impurities may be lower molecular weight proteins or other molecules with affinity to some components of the packed columns (e.g., nickel or agarose) that were eluted during the imidazole gradient at the same imidazole concentration as the GnFt nanoparticles.

Mass photometry confirmed that GnFt nanoparticles from both purification strategies contained the expected 24-mer oligomeric form with an approximate molecular weight of 1,344 kDa (Fig. 3E).

Together, these results indicate that pure GnFt nanoparticles can be obtained by dialysis of culture supernatants followed by ProteIndex cartridge purification (i.e., TC strategy). If using direct loading onto the cartridges (i.e., DL strategy), an additional subsequent size-exclusion chromatography step must be performed to remove the higher molecular weight impurities.

The purified GnFt nanoparticles obtained with the TC approach were compared to ferritin (Ft) nanoparticles lacking the Gn antigen. Reducing SDS-PAGE showed the expected Ft monomers with a molecular weight of 20 kDa (Fig. 4A), while assembled 24-mer Ft nanoparticles displayed a mass of ~500 kDa, as confirmed by mass photometry (Fig. 4B). DLS analysis revealed a clear hydrodynamic diameter shift between Gn-presenting (~20 nm) and non-presenting (~12 nm) Ft nanoparticles (Fig. 4C). Furthermore, nsTEM analysis showed globular, round-shaped Ft nanoparticles with a smooth surface with a diameter of less than 14 nm, while GnFt displayed well-assembled nanoparticles with distinct surrounding densities characteristic of Gn antigens and a diameter of ~18 nm (Fig. 4D). Because DLS estimates the hydrodynamic diameter, the irregular shape caused by the fused antigens may have contributed to a larger hydrodynamic

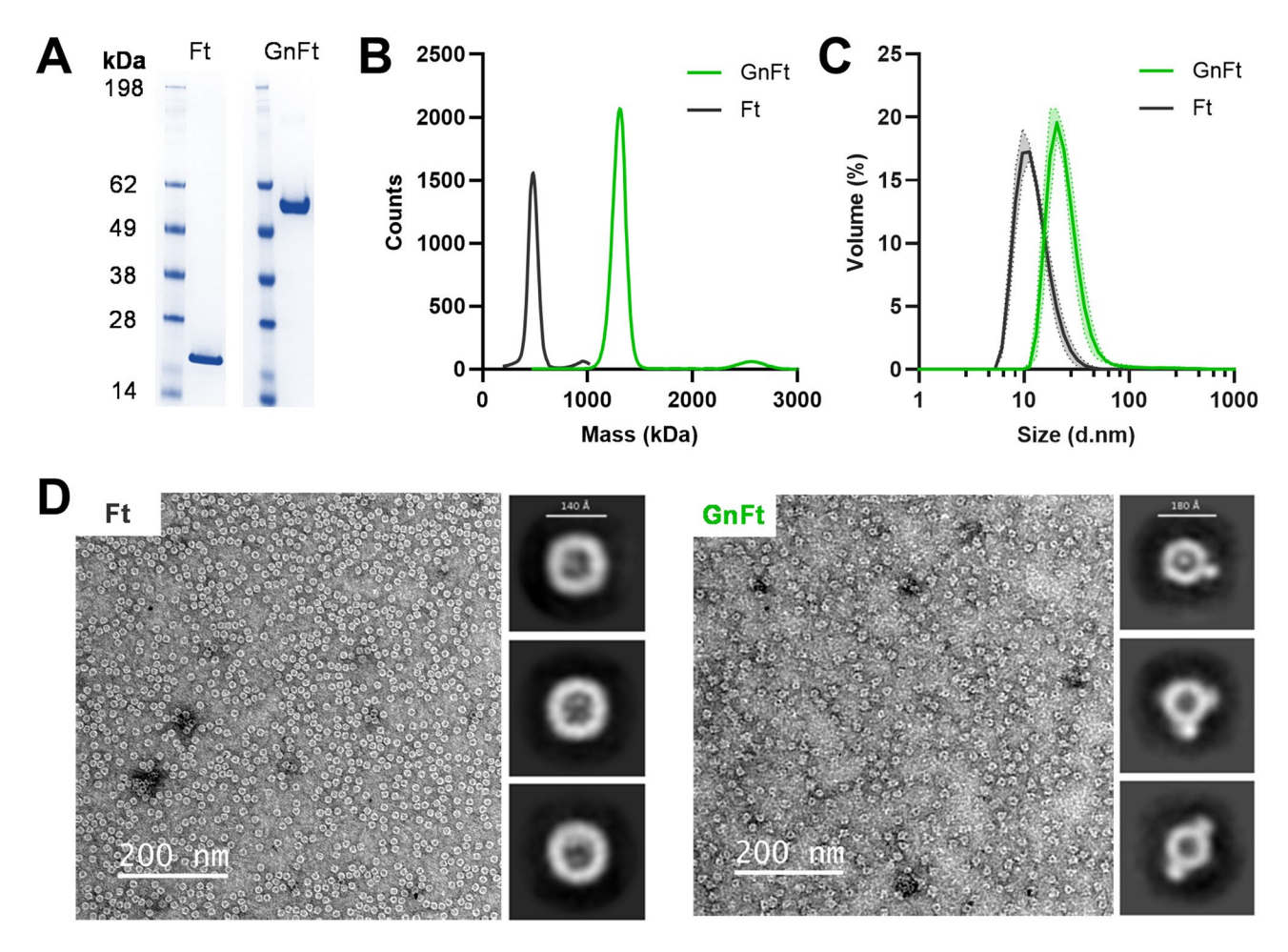


Fig. 4 Comparison of purified GnFt and Ft nanoparticles. (**A-D**) Characterization of purified Ft (grey) and GnFt (green) nanoparticles. (**A**) SDS-PAGE analysis of Ft (20 kDa) and GnFt (56 kDa); wells contain 1 μg of protein. (**B**) Molecular weight estimation by mass photometry. (**C**) Particle size distribution by DLS. Data represents mean ± SD from n = 3 technical replicates. Corresponding correlograms are presented in Fig. S7B. (**D**) Representative nsTEM micrographs of Ft (left) and GnFt (right) nanoparticles with 2D classes depicted on the right. Scale bars of the 2D classes represent 140 Å and 180 Å for Ft and GnFt nanoparticles, respectively

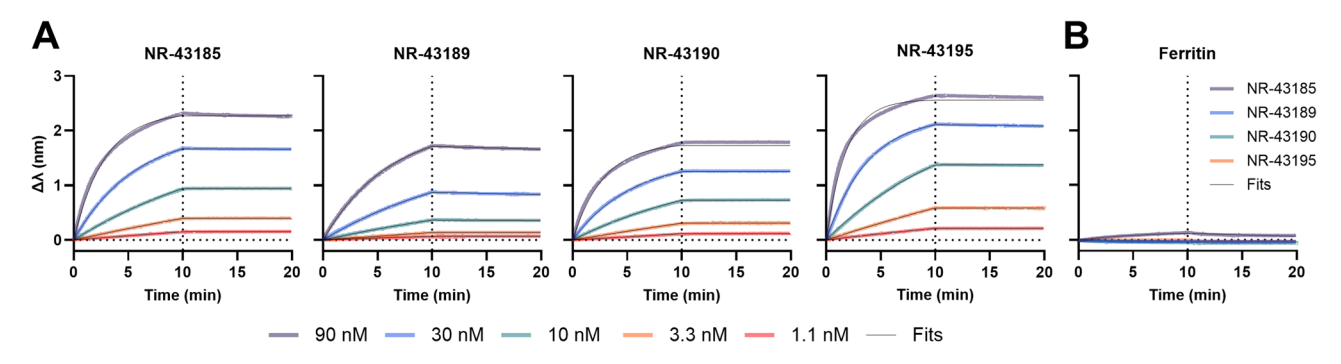


Fig. 5 Comparison of purified GnFt and Ft nanoparticles. (**A**) BLI sensorgrams showing real-time binding kinetics of four RVFV Gn-specific monoclonal antibodies (NR-43185, NR-43189, NR-43195) used at threefold serial dilutions, starting at 90 nM, to GnFt nanoparticles. (**B**) BLI sensorgram of Ft nanoparticles using 90 nM of each antibody as single concentration

radius than that estimated by nsTEM. In summary, GnFt nanoparticles were successfully produced in *Sf*9 cells and purified to yield structurally stable and pure nanoparticles suitable for further applications.

To assess the antigenic integrity of Gn presented on the nanoparticle surface, biolayer interferometry (BLI) was performed using four RVFV Gn-specific monoclonal antibodies (NR-43185, NR-43189, NR-43190, and NR-43195), the latter two being neutralizing (Fig. 5A).

Table 2 Binding kinetics of RVFV Gn-specific monoclonal antibodies to GnFt nanoparticles. Equilibrium dissociation constants (K_D), association rate constants (K_{on}), and dissociation rate constants (K_{off}) were determined by nonlinear regression analysis of BLI sensorgrams

Antibody ID	k _{on} (×10 ⁶ M ⁻¹ .min ⁻¹)	$k_{off} (\times 10^{-2} M^{-1}.min^{-1})$	K _D (nM)
NR-43185	0.74	6.66	1.11
NR-43189	0.15	2.77	0.55
NR-43190	0.59	7.06	0.83
NR-43195	1.11	9.12	1.21

Association and dissociation kinetics were recorded in real time and fit to a nonlinear regression. All antibodies bound GnFt with equilibrium dissociation constants (K_D) in the nanomolar range (Table 2), indicating high-affinity interactions and preservation of conformational epitopes. No significant binding was detected to Gn-devoid Ft nanoparticles, confirming the specificity of antibody recognition (Fig. 5B).

Discussion

Selecting suitable expression systems and designing scalable bioprocesses are critical for biopharmaceutical production. Baculoviruses are well-suited for these tasks as they can be easily constructed and amplified to high titers using insect cells with minimal safety concerns [17]. Additionally, IC-BEVS is an established method, with several commercially available products, supporting regulatory acceptance of baculovirus-derived biotherapeutics.

Given the potential for ferritin-based vaccines and the urgent need for RVFV prophylaxis, we designed a ferritin nanoparticle fused to the immunogenic ectodomain of RVFV Gn. Through a series of optimization experiments, we sought to establish a bioprocess to produce GnFt nanoparticles using a baculovirus-based expression system.

Baculoviruses can be used in both insect and mammalian cell lines, being valuable for high-throughput screening assays where mammalian systems fall short [31]. Insect cells lack the ability to perform complex post-translational modifications such as sialylation, essential for the functionality of many pharmaceutical proteins. The lytic nature of IC-BEVS presents further challenges, including protease release and incomplete protein processing [46], as well as premature cell death that hinders continuous production, although multistage bioreactor strategies may offer solutions [47]. These challenges contributed to the development of BacMam.

In mammalian cells, baculoviruses offer advantages over plasmid DNA-based transient expression, which is inefficient and costly. Studies have shown that transduction with rBAC is superior to transfection agents [48], and BacMam expression levels surpass those achieved

with calcium phosphate co-precipitation or lipofection [18, 49], especially when using transcription enhancers [48]. In contrast to viral vectors like adenoviruses and adeno-associated viruses, which have limited scalability and capacity (< 8 kb), BacMam provides greater scalability and can accommodate larger constructs (~ 80 kb), ideal for producing complex, multicomponent proteins [50]. While adenoviral transfection showed higher efficiency, BacMam achieved comparable expression levels [18]. Additionally, BacMam's non-replicative nature allows for continuous production. For example, Jardin et al. sustained HEK cell expression for up to 30 days using a semi-continuous perfusion process with a hollow fiber bioreactor system [51].

In this work, initial tests with BacMam showed no apparent expression in CHO cells, consistent with previous reports that CHO cells require higher baculoviral dosages compared to HEK [48], with rBAC transduction efficiency in CHO being poor [46] and less effective than in HEK cells, where expression was at least 10-fold higher [51]. BacMam rBAC stocks formulated in insect cell medium led to HEK293 cell death, consistent with findings that Sf900III medium induces high cell aggregation and severely compromises viability [52]. To address this, previous studies either changed the cell culture medium after viral addition or prepared viral stocks in different formulations, as insect cell media can interfere with mammalian baculoviral transduction [51]. Puente-Massaguer et al. used rBAC stocks in FreeStyle 293 medium, which still led to cell clumping and viability decrease, albeit to a lesser extent [52]. Transduction in PBS proved more efficient [53, 54] and yielded higher expression levels compared to using insect or mammalian media [54]. In this work, medium exchange after viral addition showed no detrimental effect to productivity or cell growth, while the use of concentrated virus formulated in PBS minimized the volume of rBAC stock needed to obtain the high MOIs required for BacMam [51].

Various MOIs and cell concentrations at transduction were tested for optimal productivity, as these critical process parameters are cell- and product-dependent. Using a Design of Experiments (DOE) approach, Jardin et al. found that MOI and the synergy between MOI and cell concentration at transduction most impacted transduction and secreted alkaline phosphatase levels, with a MOI of 500 pfu/cell being optimal [51]. Miyaushi et al. reported peak expression of drug-metabolizing enzymes at MOIs of 75-100 pfu/cell [49], while for virus-like particle (VLP) production, Tang et al. observed increased expression with higher MOIs, saturating at MOI > 60 pfu/ cell [53]. Using DOE, Puente-Massaguer et al. selected an optimal MOI of 50 pfu/cell and cell concentration at transduction of 2×10^6 cells/mL for VLP production [52]. Combining high MOIs with high cell concentrations led to widespread cell aggregation [52], while MOIs of 400–800 pfu/cell hampered cell growth, postulated to be due to viral genome overloading and subsequent overexpression-related toxicity and metabolic burden. Hu et al. selected MOI of 200 pfu/cell as optimal for GFP production [46]. In this work, GnFt production in HEK293 cells using MOI of 25 pfu/cell and cell concentration at transduction of 2×10^6 cells/mL were considered optimal. Although the selected cell concentration is consistent with the literature, higher MOIs could improve productivity, and the use of a DOE approach could help streamline various variables that synergistically influence final yields.

Histone deacetylase inhibitors are commonly used to upregulate gene expression. GnFt expression was improved 3- to 4-fold using 1 mM NaBut, which was chosen over 5 mM due to cytotoxicity. Prior studies found optimal NaBut concentrations in the 3-4.5 mM range, with associated cytotoxicity [49], while others reported 5–7 mM for VLP production [52, 53]. Valproate is a less cytotoxic alternative, though less effective [46], and trichostatin A (TSA) also enhances expression [51]. Notably, Toth et al. found that NaBut or TSA can be used at lower molarities (μM and nM) maintaining high expression, minimizing cytotoxicity, and offering a more cost-effective scale-up [48].

BacMam could be further improved using a low-pH trigger [55] (e.g., Ouabain), which decreases the pH of early endosomes and enhances virus transduction in several mammalian cells [54]. Additionally, since rBAC primarily enters through clathrin-mediated endocytosis (a low pH-dependent endocytic pathway), inhibiting other pathways, such as using the caveolar endocytosis inhibitor genistein, can significantly enhance cell transduction [56]. Further strategies could include lowering the temperature to 27 °C upon viral addition to preserve the physical integrity of rBAC [54], or using vesicular stomatitis virus glycoprotein (VSVG)-containing rBAC to increase baculoviral escape from intracellular vesicles [57].

Although IC-BEVS is a well-established expression platform that leverages the native machinery of baculovirus infection and amplification to achieve high expression levels, infection conditions must still be optimized based on the cell line and product being expressed.

The *Sf9*-derived Super*Sf9* cell line, engineered for enhanced expression, has shown higher expression levels of the Spike protein from SARS-CoV2 compared to *Sf9* [58], but lower expression for an antigen derived from the malaria-causing agent *Plasmodium falciparum* [59]. In this work, Super*Sf9* was the least efficient cell line for GnFt expression.

*Tn*ms42 [33, 34] and *Tn*ao38 [35, 36], described as being adventitious virus-free cell lines, are more suitable

for biologics manufacturing than benchmark cell lines, such as Sf9 and Hi5, which harbour rhabdovirus and nodavirus, respectively (reviewed in [60]). Although these viruses are non-infectious in mammalian cells [60], their presence can pose safety concerns and regulatory barriers. Several reports have used Tnms42 for VLP production [61-63]. In this work, GnFt expression was less efficient in *Tn*ms42 compared to *Sf*9, Hi5, and *Tn*ao38. Notably, Tnao38 demonstrated expression levels comparable to Sf9 and Hi5, making it a promising candidate for biologics manufacturing, as also reported by Wilde et al. [64]. Both Tnms42 and Tnao38 displayed a slower infection profile and higher VCDs, consequently leading to lower cell-specific productivities. This may be due to suboptimal medium adaptation at the time of the experiments; using optimized media for these cell lines could enhance productivities. Based on these findings, Sf9 and Hi5 were identified as the most suitable GnFt producers using IC-BEVS.

The GnFt nanoparticles were designed with a histidine tag to enable purification via IMAC using nickel-charged resins. The evaluation of GnFt purification in HEK293, Hi5, and Sf9 cells using His. Bind resin highlighted differences in host-dependent production. Despite production optimization efforts, GnFt from HEK293 and Hi5 cells remained mostly intracellular, making purification challenging. This suggests potential limitations in secretion efficiency or GnFt stability in these systems. In contrast, Sf9 cells enabled efficient secretion and high-affinity purification, leading to pure nanoparticles. These results indicate that Sf9 cells offer a more suitable platform for GnFt production, ensuring sufficient yield and purity for further development. This comparative analysis further reinforces the importance of selecting an appropriate host for antigen-fused ferritin nanoparticle production.

With Sf9 cells identified as the most suitable production platform, the following step was to optimize purification conditions to ensure efficient recovery of GnFt nanoparticles. Since eukaryotic culture media can interfere with protein binding or cause nickel leakage, it is recommended to dialyze culture supernatants against compatible buffers before loading onto conventional columns. Malvergent's ProteIndex Ni-Penta prepacked cartridges offer a chemically stable structure that minimizes nickel leakage, even under harsh conditions such as detergent-containing lysates or cell culture supernatants. This technology reduces the need for frequent regeneration, simplifying bioprocesses, and improving scalability while minimizing the wastage of toxic heavy metals. Both treated or direct load of clarified supernatants onto ProteIndex Ni-Penta yielded GnFt nanoparticles of the expected size and molecular weight. However, the treated clarified approach yielded the most favourable outcome, producing GnFt nanoparticles with >95%

purity; these particles can be polished by means of size exclusion chromatography (e.g., Superose 6) in order to obtain a product of sufficient purity to advance to clinical trials. Direct loading of clarified supernatants resulted in purified material containing large particles and/or impurities, highlighting the importance of buffer-exchange for removing media components that reduce the performance of ProteIndex cartridges.

Given the design of GnFt as a chimeric protein, the histidine tag was utilized to facilitate protein identification in cell culture bulk samples during expression assays and enable purification by means of nickel-charged affinity chromatography. For vaccine development purposes, future work should integrate a cleavage site downstream of the histidine tag (e.g., TEV cleavage site), or preferably, establish ion exchange chromatography followed by polishing by size exclusion chromatography, which is the most commonly used purification workflow to purify such products [65–70].

Genetic fusion constructs of ferritin with complex antigens are often produced in high order eukaryotes to enable post-translational modifications and prevent the refolding challenges associated with bacterial inclusion bodies. In this work, the yield of GnFt nanoparticle expression was 0.2 mg/mL using the Sf9-baculovirus expression system. This expression can be improved by adding supplements (e.g., reduced glutathione, antioxidants) and implementing high-cell density culture strategies (e.g., perfusion bioreactor) which have been shown to improve VLP and recombinant protein production [71–73]. Given that a portion of protein still remained intracellular, purification of the total cell culture could yield more protein. Selecting a different expression system and host could also improve GnFt expression. For example, plasmid-based transfection of HEK293 yielded ferritin-based nanoparticle vaccines in the range of 0.5-10 mg/mL [8, 12, 74-76]. CHO cells have emerged as a superior expression system for producing antigen-fused ferritin nanoparticles with complex structures, yielding up to 20-40 times more product compared to HEK cells [75, 77]. Products derived from CHO cells also exhibited superior nanoparticle assembly and homogeneity [78]. Notably, Weidenbacher et al. [69] reported stable CHO K1 cell lines achieving yields > 2 g/L, representing a significant advancement over transient mammalian expression methods. Also worth mentioning is the silkworm system, with demonstrated yields of 0.2–1 g/L [79, 80].

To consider Sf9 cells and the GnFt nanoparticle platform as a viable RVF vaccine candidate, several key parameters must be met. Expression titers in the range of $\geq 1-10$ mg/L are required to support preclinical studies, with titers exceeding 100 mg/L being preferable for large-scale manufacturing. The production timeline should allow for batch readiness within 10-14 days to

ensure responsiveness in outbreak scenarios. Immunogenicity studies must demonstrate the induction of robust and durable immune responses, including virus-neutralizing antibody production in relevant animal models (e.g., mice, non-human primates), while achieving neutralizing antibody titers in the range demonstrated by ferritin-based vaccines for other viral pathogens, typically $> 10^3 - 10^4$ GMT [8, 12, 77]. The platform should also be compatible with established bioprocessing workflows, including scalable and regulatory-compliant purification strategies, as demonstrated in this work. Finally, cost must be kept low to support broad accessibility and rapid deployment, particularly in low-resource settings. In this context, insect cell-baculovirus systems may offer a more cost-effective alternative to plasmid-based transient expression and lentivirus-based stable expression in mammalian cells, as they eliminate the need for transfection reagents, high-cost DNA preparations, and lengthy cell line development, while supporting suspension growth in serum-free media and enabling rapid scalability.

The comparison between GnFt and Ft nanoparticles highlights the structural impact of Gn antigen display on ferritin assembly. The observed hydrodynamic diameter and molecular weight shifts in DLS and mass photometry analysis, alongside the distinct surrounding densities in nsTEM, confirms the successful presentation of Gn on the nanoparticle surface without compromising proper nanoparticle assembly. The consistency between mass photometry and SDS-PAGE further validates the structural integrity of both monomeric and assembled forms. Additionally, BLI experiments confirmed the retained functionality of the displayed Gn domain, as evidenced by specific binding to Gn-targeting monoclonal antibodies with high affinities, supporting the conformational integrity of the antigen and its accessibility on the nanoparticle surface. All things considered, these results support the suitability of using Sf9 cells and affinity chromatography as a platform for GnFt nanoparticles production and purification, providing a solid basis for future immunostimulatory studies.

Conclusions

This study establishes a platform for the production and purification of GnFt nanoparticles, demonstrating the suitability of *Sf*9 cells and the baculovirus expression vector system for generating stable and well-assembled antigen-presenting nanoparticles. The systematic evaluation of expression hosts, purification strategies, and nanoparticle physico-chemical characterization provides a strong basis for optimizing recombinant ferritin-based vaccines. Future work will focus on increasing yields and assessing the immunogenic properties of GnFt nanoparticles

to further explore their potential in vaccine development for RVF.

Abbreviations

BacMam Baculovirus transduction of mammalian cells

BLI Biolayer interferometry bPRL Bovine prolactin

CCI Cell concentration at infection
CHO Chinese hamster ovary cells
CMV Cytomegalovirus
DLS Dynamic light scattering

EGFP Enhanced green fluorescent protein

Ft Ferritin

Gn Gn domain of Rift Valley fever virus envelope glycoprotein

GnFt Gn-fused ferritin

GP67 Autographa californica nuclear polyhedrosis virus major

envelope glycoprotein

hCD5 human cluster of differentiation 5 HEK Human embryonic kidney cells

hpi hours post infection

HPLC High performance liquid chromatography IC-BEVS Insect cells-baculovirus expression vector system

IL2 Human interleukin-2 IMAC Immobilized metal affinity chromatography

MOI Multiplicity of infection

nsTEM negative staining transmission electron microscopy

PGK human phosphoglycerate kinase

PH Polyhedrin

rBAC recombinant baculovirus RVFV Rift Valley fever virus

SDS-PAGE Sodium dodecyl-sulphate polyacrylamide gel electrophoresis

TFF Tangential flow filtration
TOH Time of harvest
VCD Viable cell density
VLP Virus-like particles

Supplementary Information

The online version contains supplementary material available at https://doi.org/10.1186/s13036-025-00550-8.

Supplementary Material 1

Acknowledgements

The authors acknowledge Tiago Nunes from the Late-Stage R&D and Bioproduction Unit at iBET for the support in HPLC analysis, and the Electron Microscopy Facility at CIC bioGUNE for sample preparation and TEM analysis. The vector pRRLSIN.cPPT.PGK-GFP.WPRE was a gift from Didier Trono (Addgene plasmid #12252). The following reagents were obtained from the Joel M. Dalrymple – Clarence J. Peters USAMRIID Antibody Collection through BEI Resources, NIAID, NIH: Monoclonal Anti-Rift Valley Fever Virus Gn Glycoprotein, NR-43185 (Clone 7B6), NR-43189 (Clone 3D11), NR-43190 (Clone 4D4), and NR-43195 (Clone 4-39-CC) (all produced in vitro). Graphical abstract was developed with BioRender.com, with molecular structures obtained using UCSF ChimeraX, developed by the Resource for Biocomputing, Visualization, and Informatics at the University of California, San Francisco, with support from NIH R01-GM129325 and the Office of Cyber Infrastructure and Computational Biology, NIAID.

Author contributions

M.Q.R. conceived the idea and designed the study. M.Q.R and B.K. were involved in vector cloning and protein purification. M.Q.R. and A.B.T. performed protein production, purification, and characterization. M.Q.R. wrote the original-draft. P.M.A. and A.R. contributed to funding acquisition, supervision, and manuscript review and editing.

Funding

The authors acknowledge the support from European Commission through the project "PROMETEUS" (grant number 823780), from Portuguese Fundação para a Ciência e a Tecnologia (FCT) through the PhD fellowship (DFA/

BD/8167/2020), and from FEDER and National Funds through the project "eZVac" (LISBOA2030-FEDER-00754700, Project ID 16381). The Research Unit UID/04462: iNOVA4Health – Programme in Translational Medicine, financially supported by FCT/Ministério da Educação, Ciência e Inovação and the Associate Laboratory LS4FUTURE (LA/P/0087/2020) are acknowledged.

Data availability

The datasets used and/or analysed during the current study are available from the corresponding author on reasonable request.

Declarations

Ethics approval and consent to participate

Not applicable.

Consent for publication

All authors agree to publication.

Competing interests

The authors declare no competing interests.

Author details

¹Instituto de Biologia Experimental e Tecnológica, Apartado 12,

Oeiras 2781-901, Portugal

²Instituto de Tecnologia Química e Biológica António Xavier, ITQB NOVA, Universidade Nova de Lisboa, Av. da República, Oeiras 2780-157, Portugal ³Department of Physiology and Cellular Biophysics, Columbia University Vagelos College of Physicians and Surgeons, New York, NY 10032, USA

Received: 13 June 2025 / Accepted: 8 August 2025

Published online: 14 August 2025

References

- Smith DM, Simon JK, Baker JR Jr. Applications of nanotechnology for immunology. Nat Rev Immunol. 2013;13:592–605.
- Foged C, Brodin B, Frokjaer S, Sundblad A. Particle size and surface charge affect particle uptake by human dendritic cells in an in vitro model. Int J Pharm. 2005;298:315–22.
- 3. Rodrigues MQ, Alves PM, Roldão A. Functionalizing ferritin nanoparticles for vaccine development. Pharmaceutics. 2021;13:1621.
- Zakeri B, Fierer JO, Celik E, Chittock EC, Schwarz-Linek U, Moy VT, et al. Peptide Tag forming a rapid covalent bond to a protein, through engineering a bacterial adhesin. Proc Natl Acad Sci. 2012;109:E690–7.
- Kolb HC, Finn MG, Sharpless KB. Click chemistry: diverse chemical function from a few good reactions. Angew Chem Int Ed. 2001;40:2004–21.
- Rodrigues MQ, Patão S, Thomaz M, Nunes T, Alves PM, Roldão A. Tyrosinase-Mediated conjugation for antigen display on ferritin nanoparticles. Bioconjug Chem. 2024;35:1608–17.
- Li CQ, Soistman E, Carter DC. Ferritin nanoparticle technology... A new platform for antigen presentation and vaccine development. Ind Biotechnol. 2006:2:143–7.
- Kanekiyo M, Wei C-J, Yassine HM, McTamney PM, Boyington JC, Whittle JRR, et al. Self-assembling influenza nanoparticle vaccines elicit broadly neutralizing H1N1 antibodies. Nature. 2013;499:102–6.
- Yassine HM, Boyington JC, McTamney PM, Wei C-J, Kanekiyo M, Kong W-P, et al. Hemagglutinin-stem nanoparticles generate heterosubtypic influenza protection. Nat Med. 2015;21:1065–70.
- Houser KV, Chen GL, Carter C, Crank MC, Nguyen TA, Burgos Florez MC, et al. Safety and immunogenicity of a ferritin nanoparticle H2 influenza vaccine in healthy adults: a phase 1 trial. Nat Med. 2022;28:383–91.
- Kanekiyo M, Bu W, Joyce MG, Meng G, Whittle JRR, Baxa U, et al. Rational design of an Epstein-Barr virus vaccine targeting the Receptor-Binding site. Cell. 2015;162:1090–100.
- Joyce MG, Chen W-H, Sankhala RS, Hajduczki A, Thomas PV, Choe M, et al. SARS-CoV-2 ferritin nanoparticle vaccines elicit broad SARS coronavirus immunogenicity. Cell Rep. 2021;37:110143.
- Saunders KO, Wiehe K, Tian M, Acharya P, Bradley T, Alam SM, et al. Targeted selection of HIV-specific antibody mutations by engineering B cell maturation. Science. 2019;366:eaay7199.

- Kim Y-S, Son A, Kim J, Kwon SB, Kim MH, Kim P, et al. Chaperna-Mediated assembly of Ferritin-Based middle East respiratory Syndrome-Coronavirus nanoparticles. Front Immunol. 2018;9:1093.
- Monie A, Hung C-F, Roden R, Wu T-C. Cervarix [™]: a vaccine for the prevention of HPV 16, 18-associated cervical cancer. Biol Targets Ther. 2008;2:107–13.
- Cox MMJ, Izikson R, Post P, Dunkle L. Safety, efficacy, and immunogenicity of Flublok in the prevention of seasonal influenza in adults. Ther Adv Vaccines. 2015;3:97–108.
- Chen C-Y, Lin C-Y, Chen G-Y, Hu Y-C. Baculovirus as a gene delivery vector: recent Understandings of molecular alterations in transduced cells and latest applications. Biotechnol Adv. 2011;29:618–31.
- Hofmann C, Sandig V, Jennings G, Rudolph M, Schlag P, Strauss M. Efficient gene transfer into human hepatocytes by baculovirus vectors. Proc Natl Acad Sci. 1995;92:10099–103.
- 19. Flick R, Bouloy M. Rift Valley fever virus. Curr Mol Med. 2005;5:827-34.
- Grobbelaar AA, Weyer J, Leman PA, Kemp A, Paweska JT, Swanepoel R. Molecular epidemiology of rift Valley fever virus. Emerg Infect Dis. 2011;17:2270–6.
- 21. Alhaj M. Safety and efficacy profile of commercial veterinary vaccines against rift Valley fever: A review study. J Immunol Res. 2016;2016:7346294.
- Kitandwe PK, McKay PF, Kaleebu P, Shattock RJ. An overview of rift Valley fever vaccine development strategies. Vaccines. 2022;10:1794.
- Suzich JA, Kakach LT, Collett MS. Expression strategy of a phlebovirus: biogenesis of proteins from the rift Valley fever virus M segment. J Virol. 1990;64:1549–55.
- Wright D, Allen ER, Clark MHA, Gitonga JN, Karanja HK, Hulswit RJG, et al. Naturally acquired rift Valley fever virus neutralizing antibodies predominantly target the Gn glycoprotein. iScience. 2020;23:101669.
- Trikha J, Theil EC, Allewell NM. High resolution crystal structures of amphibian Red-Cell L ferritin: potential roles for structural plasticity and solvation in function. J Mol Biol. 1995;248:949–67.
- Cho KJ, Shin HJ, Lee J-H, Kim K-J, Park SS, Lee Y, et al. The crystal structure of ferritin from *Helicobacter pylori* reveals unusual conformational changes for iron uptake. J Mol Biol. 2009;390:83–98.
- 27. Collett MS, Purchio AF, Keegan K, Frazier S, Hays W, Anderson DK, et al. Complete nucleotide sequence of the M RNA segment of rift Valley fever virus. Virology. 1985;144:228–45.
- Wichgers Schreur PJ, Tacken M, Gutjahr B, Keller M, van Keulen L, Kant J, et al. Vaccine efficacy of Self-Assembled multimeric protein scaffold particles displaying the glycoprotein Gn head domain of rift Valley fever virus. Vaccines. 2021:9:301.
- Aslanidis C, de Jong PJ. Ligation-independent cloning of PCR products (LIC-PCR). Nucleic Acids Res. 1990;18:6069–74.
- Kloss B. Genomics-based strategies toward the identification of a Z-ISO carotenoid biosynthetic enzyme suitable for structural studies. Methods Enzymol. 2022;671:171–205.
- Goehring A, Lee C-H, Wang KH, Michel JC, Claxton DP, Baconguis I, et al. Screening and large-scale expression of membrane proteins in mammalian cells for structural studies. Nat Protoc. 2014;9:2574–85.
- Luckow VA, Lee SC, Barry GF, Olins PO. Efficient generation of infectious Recombinant baculoviruses by site-specific transposon-mediated insertion of foreign genes into a baculovirus genome propagated in Escherichia coli. J Virol. 1993;67:4566–79.
- Chen Y-R, Zhong S, Fei Z, Hashimoto Y, Xiang JZ, Zhang S, et al. The transcriptome of the baculovirus autographa Californica multiple nucleopolyhedrovirus in trichoplusia Ni cells. J Virol. 2013;87:6391–405.
- Chen Y-R, Zhong S, Fei Z, Gao S, Zhang S, Li Z, et al. Transcriptome responses
 of the host trichoplusia Ni to infection by the baculovirus autographa Californica multiple nucleopolyhedrovirus. J Virol. 2014;88:13781–97.
- Hashimoto Y, Zhang S, Blissard GW. Ao38, a new cell line from eggs of the black Witch moth, Ascalapha odorata (Lepidoptera: Noctuidae), is permissive for AcMNPV infection and produces high levels of recombinant proteins. BMC Biotechnol. 2010;10:50.
- Hashimoto Y, Zhang S, Zhang S, Chen Y-R, Blissard GW. Erratum to: BTI-Tnao38, a new cell line derived from trichoplusia ni, is permissive for AcMNPV infection and produces high levels of Recombinant proteins. BMC Biotechnol. 2012;12:12
- 37. Mena JA, Ramírez OT, Palomares LA. Titration of Non-Occluded baculovirus using a cell viability assay. Biotechniques. 2003;34:260–4.
- Roldão A, Oliveira R, Carrondo MJT, Alves PM. Error assessment in Recombinant baculovirus titration: evaluation of different methods. J Virol Methods. 2009;159:69–80.

- Gasteiger E. ExPASy: the proteomics server for in-depth protein knowledge and analysis. Nucleic Acids Res. 2003;31:3784–8.
- Keegan K, Collett MS. Use of bacterial expression cloning to define the amino acid sequences of antigenic determinants on the G2 glycoprotein of rift Valley fever virus. J Virol. 1986;58:263–70.
- Schneider CA, Rasband WS, Eliceiri KW. NIH image to imageJ: 25 years of image analysis. Nat Methods. 2012;9:671–5.
- Punjani A, Rubinstein JL, Fleet DJ, Brubaker MA. CryoSPARC: algorithms for rapid unsupervised cryo-EM structure determination. Nat Methods. 2017;14:290–6.
- Correia R, Fernandes B, Castro R, Nagaoka H, Takashima E, Tsuboi T, et al. Asexual Blood-Stage malaria vaccine candidate PfRipr5: enhanced production in insect cells. Front Bioeng Biotechnol. 2022;10:908509.
- Kumar N, Gammell P, Meleady P, Henry M, Clynes M. Differential protein expression following low temperature culture of suspension CHO-K1 cells. BMC Biotechnol. 2008;8:42.
- Lin C-Y, Huang Z, Wen W, Wu A, Wang C, Niu L. Enhancing protein expression in HEK-293 cells by Lowering culture temperature. PLoS ONE. 2015:10:e0123562.
- Hu Y-C, Tsai C-T, Chang Y-J, Huang J-H. Enhancement and prolongation of Baculovirus-Mediated expression in mammalian cells: focuses on strategic infection and feeding. Biotechnol Prog. 2003;19:373–9.
- 47. Correia R, Zotler T, Ferraz F, Fernandes B, Graça M, Pijlman GP et al. Continuous Production of Influenza VLPs Using IC-BEVS and Multi-Stage Bioreactors. Biotechnol Bioeng [Internet]. [cited 2025 Mar 1];n/a. Available from: https://onlinelibrary.wiley.com/doi/abs/https://doi.org/10.1002/bit.28925
- 48. Toth M, Reithofer M, Dutra G, Pereira Aguilar P, Dürauer A, Grabherr R. Comprehensive comparison of baculoviral and plasmid gene delivery in mammalian cells. Viruses. 2024;16:426.
- Miyauchi Y, Kimura A, Sawai M, Fujimoto K, Hirota Y, Tanaka Y, et al. Use of a Baculovirus-Mammalian cell expression-System for expression of Drug-Metabolizing enzymes: optimization of infection with a focus on cytochrome P450 3A4. Front Pharmacol. 2022;13:832931.
- Zhai Y, Zhang D, Yu L, Sun F, Sun F. SmartBac, a new baculovirus system for large protein complex production. J Struct Biol X. 2019;1:100003.
- Jardin B, Zhao Y, Selvaraj M, Montes J, Tran R, Prakash S, et al. Expression of SEAP (secreted alkaline phosphatase) by baculovirus mediated transduction of HEK 293 cells in a Hollow fiber bioreactor system. J Biotechnol. 2008;135:272–80.
- Puente-Massaguer E, Cajamarca-Berrezueta B, Volart A, González-Domínguez I, Gòdia F. Transduction of HEK293 cells with BacMam baculovirus is an efficient system for the production of HIV-1 Virus-like particles. Viruses. 2022;14:636.
- 53. Tang X-C, Lu H-R, Ross TM. Baculovirus-Produced influenza Virus-like particles in mammalian cells protect mice from lethal influenza challenge. Viral Immunol. 2011;24:311–9.
- Hu L, Li Y, Ning Y-J, Deng F, Vlak JM, Hu Z et al. The Major Hurdle for Effective Baculovirus Transduction into Mammalian Cells Is Passing Early Endosomes. Shisler JL, editor. J Virol. 2019;93:e00709-19.
- Dong S, Wang M, Qiu Z, Deng F, Vlak JM, Hu Z, et al. Autographa Californica multicapsid nucleopolyhedrovirus efficiently infects Sf9 cells and transduces mammalian cells via direct fusion with the plasma membrane at low pH. J Virol. 2010;84:5351–9.
- Long G, Pan X, Kormelink R, Vlak JM. Functional entry of baculovirus into insect and mammalian cells is dependent on Clathrin-Mediated endocytosis. J Virol. 2006;80:8830–3.
- 57. Barsoum J, Brown R, McKee M, Boyce FM. Efficient transduction of mammalian cells by a Recombinant baculovirus having the vesicular stomatitis virus G glycoprotein. Hum Gene Ther. 1997;8:2011–8.
- Fernandes B, Castro R, Bhoelan F, Bemelman D, Gomes RA, Costa J, et al. Insect cells for High-Yield production of SARS-CoV-2 Spike protein: Building a Virosome-Based COVID-19 vaccine candidate. Pharmaceutics. 2022;14:854.
- Lee S-M, Plieskatt J, Krishnan S, Raina M, Harishchandra R, King CR. Expression and purification optimization of an N-terminal Pfs230 transmission-blocking vaccine candidate. Protein Expr Purif. 2019;160:56–65.
- Geisler C, Jarvis DL. Adventitious viruses in insect cell lines used for Recombinant protein expression. Protein Expr Purif. 2018;144:25–32.
- Klausberger M, Leneva IA, Egorov A, Strobl F, Ghorbanpour SM, Falynskova IN, et al. Off-target effects of an insect cell-expressed influenza HA-pseudotyped Gag-VLP Preparation in limiting postinfluenza Staphylococcus aureus infections. Vaccine. 2020;38:859–67.

- Strobl F, Ghorbanpour SM, Palmberger D, Striedner G. Evaluation of screening platforms for virus-like particle production with the baculovirus expression vector system in insect cells. Sci Rep. 2020;10:1065.
- 63. Reiter K, Pereira Aguilar P, Grammelhofer D, Joseph J, Steppert P, Jungbauer A. Separation of influenza virus-like particles from baculovirus by polymergrafted anion exchanger. J Sep Sci. 2020;43:2270–8.
- Wilde M, Klausberger M, Palmberger D, Ernst W, Grabherr R. Tnao38, high five and Sf9—evaluation of host-virus interactions in three different insect cell lines: baculovirus production and Recombinant protein expression. Biotechnol Lett. 2014;36:743–9.
- Kim D, Kim E, Kim S, Chung Y, Lai C-J, Cha I, et al. Self-assembling Gn head ferritin nanoparticle vaccine provides full protection from lethal challenge of Dabie bandavirus in aged ferrets. mBio. 2023;14:e01868–23.
- Pattnaik A, Sahoo BR, Struble LR, Borgstahl GEO, Zhou Y, Franco R, et al. A ferritin Nanoparticle-Based Zika virus vaccine candidate induces robust humoral and cellular immune responses and protects mice from lethal virus challenge, Vaccines, 2023;11:821.
- Powell AE, Xu D, Roth GA, Zhang K, Chiu W, Appel EA, et al. Multimerization of Ebola gp∆mucin on protein nanoparticle vaccines has minimal effect on elicitation of neutralizing antibodies. Front Immunol. 2022;13:942897.
- Salinas ND, Ma R, McAleese H, Ouahes T, Long CA, Miura K, et al. A Self-Assembling Pfs230D1-Ferritin nanoparticle vaccine has potent and durable malaria Transmission-Reducing activity. Vaccines. 2024;12:546.
- Weidenbacher PA-B, Sanyal M, Friedland N, Tang S, Arunachalam PS, Hu M, et al. A ferritin-based COVID-19 nanoparticle vaccine that elicits robust, durable, broad-spectrum neutralizing antisera in non-human primates. Nat Commun. 2023:14:2149.
- Xu D, Powell AE, Utz A, Sanyal M, Do J, Patten JJ, et al. Design of universal Ebola virus vaccine candidates via Immunofocusing. Proc Natl Acad Sci U S A. 2024;121:e2316960121.
- Monteiro F, Bernal V, Chaillet M, Berger I, Alves PM. Targeted supplementation design for improved production and quality of enveloped viral particles in insect cell-baculovirus expression system. J Biotechnol. 2016;233:34–41.
- Fernandes B, Sousa M, Castro R, Schäfer A, Hauser J, Schulze K et al. Scalable Process for High-Yield Production of PfCyRPA Using Insect Cells for Inclusion in a Malaria Virosome-Based Vaccine Candidate. Front Bioeng Biotechnol

- [Internet]. 2022 [cited 2025 Jul 16];10. Available from: https://www.frontiersin.org/journals/bioengineering-and-biotechnology/articles/https://doi.org/10.3389/fbioe.2022.879078/full
- Fernandes B, Correia R, Sousa M, Carrondo MJT, Alves PM, Roldão A. Integrating high cell density cultures with adapted laboratory evolution for improved Gag-HA virus-like particles production in stable insect cell lines. Biotechnol Bioeng. 2021;118:2536–47.
- Georgiev IS, Joyce MG, Chen RE, Leung K, McKee K, Druz A, et al. Two-Component ferritin nanoparticles for multimerization of diverse trimeric antigens. ACS Infect Dis. 2018:4:788–96.
- Swanson KA, Rainho-Tomko JN, Williams ZP, Lanza L, Peredelchuk M, Kishko M, et al. A respiratory syncytial virus (RSV) F protein nanoparticle vaccine focuses antibody responses to a conserved neutralization domain. Sci Immunol. 2020;5:eaba6466–6466.
- He L, Tzarum N, Lin X, Shapero B, Sou C, Mann CJ, et al. Proof of concept for rational design of hepatitis C virus E2 core nanoparticle vaccines. Sci Adv. 20206:eaaz6225–6225.
- Powell AE, Zhang K, Sanyal M, Tang S, Weidenbacher PA, Li S, et al. A single immunization with Spike-Functionalized ferritin vaccines elicits neutralizing antibody responses against SARS-CoV-2 in mice. ACS Cent Sci. 2021;7:183–99.
- He L, de Val N, Morris CD, Vora N, Thinnes TC, Kong L, et al. Presenting nativelike trimeric HIV-1 antigens with self-assembling nanoparticles. Nat Commun. 2016;7:12041–12041.
- Li D, Song H, Li J, Liu X, Gao X, Wu T, et al. Expression and evaluation of a novel PPRV nanoparticle antigen based on ferritin Self-Assembling technology. Pharmaceutics. 2022;14:1902.
- Liu X, Song H, Jiang J, Gao X, Yi Y, Shang Y, et al. Baculovirus-expressed self-assembling SARS-CoV-2 nanoparticle vaccines targeting the S protein induce protective immunity in mice. Process Biochem Barking Lond Engl. 2023:129:200–8.

Publisher's note

Springer Nature remains neutral with regard to jurisdictional claims in published maps and institutional affiliations.